CANCER

Nicotinamide enhances natural killer cell function and yields remissions in patients with non-Hodgkin lymphoma

Frank Cichocki[1]*, Bin Zhang[1], Cheng-Ying Wu[1]†, Emily Chiu[1], Abderrahman Day[1,2], Roddy S. O'Connor[3,4], Dima Yackoubov[5], Ronit Simantov[5], David H. McKenna[6], Qing Cao[7], Todd E. Defor[7], Murali Janakiram[1]‡, Rose Wangen[1], Zuzan Cayci[8], Nathaniel Snyder[9], Akhilesh Kumar[1], Bartosz Grzywacz[6], Justin Hwang[1], Yona Geffen[5], Jeffrey S. Miller[1], Joseph Maakaron[1], Veronika Bachanova[1]*

Allogeneic natural killer (NK) cell adoptive transfer has shown the potential to induce remissions in relapsed or refractory leukemias and lymphomas, but strategies to enhance NK cell survival and function are needed to improve clinical efficacy. Here, we demonstrated that NK cells cultured ex vivo with interleukin-15 (IL-15) and nicotinamide (NAM) exhibited stable induction of L-selectin (CD62L), a lymphocyte adhesion molecule important for lymph node homing. High frequencies of CD62L were associated with elevated transcription factor forkhead box O1 (FOXO1), and NAM promoted the stability of FOXO1 by preventing proteasomal degradation. NK cells cultured with NAM exhibited metabolic changes associated with elevated glucose flux and protection against oxidative stress. NK cells incubated with NAM also displayed enhanced cytotoxicity and inflammatory cytokine production and preferentially persisted in xenogeneic adoptive transfer experiments. We also conducted a first-in-human phase 1 clinical trial testing adoptive transfer of NK cells expanded ex vivo with IL-15 and NAM (GDA-201) combined with monoclonal antibodies in patients with relapsed or refractory non-Hodgkin lymphoma (NHL) and multiple myeloma (MM) (NCT03019666). Cellular therapy with GDA-201 and rituximab was well tolerated and yielded an overall response rate of 74% in 19 patients with advanced NHL. Thirteen patients had a complete response, and 1 patient had a partial response. GDA-201 cells were detected for up to 14 days in blood, bone marrow, and tumor tissues and maintained a favorable metabolic profile. The safety and efficacy of GDA-201 in this study support further development as a cancer therapy.

INTRODUCTION

Natural killer (NK) cells are granular lymphocytes that participate in tumor immunosurveillance and control of microbial infections. They also produce proinflammatory cytokines, such as interferon-γ (IFN-γ), that shape the adaptive immune response (*1*). Previous studies of haploidentical NK cell adoptive transfer demonstrated safety and efficacy in patients with poor-prognosis acute myeloid leukemia (*2*, *3*). Haploidentical donor NK cell therapy in combination with the anti-CD20 antibody rituximab and interleukin-2 (IL-2) for the treatment of patients with poor-prognosis, refractory non-Hodgkin lymphoma (NHL) was tested in a phase 2 clinical trial. The therapy was safe, without graft-versus-host disease (GvHD), cytokine release syndrome (CRS), or neurotoxicity. However, of 14 evaluable patients, only 4 had objective responses at 2 months. Two patients achieved complete responses (CRs) lasting 3 and 9 months (*4*). Thus, new strategies are needed to enhance NK cell therapy in the lymphoma setting.

Here, we present data showing that nicotinamide (NAM) supplementation during ex vivo peripheral blood NK cell culture leads to induction of L-selectin (CD62L) that is stable in vivo after NAM withdrawal. We describe the mechanisms underpinning this finding and evaluate the effects of NAM on NK cell metabolism, function, and in vivo persistence. We also present results from a first-in-human phase 1 clinical trial evaluating adoptive transfer of NK cells expanded with NAM (GDA-201) in patients with relapsed or refractory (R/R) B cell NHL.

RESULTS

NAM prevents activation-induced loss of CD62L and induces CD62L up-regulation

Previous work demonstrated that $CD34^+$ hematopoietic progenitor cells expanded with NAM more efficiently engrafted after adoptive transfer (*5*). However, the mechanistic basis for this observation was not determined. To evaluate the effect of NAM on human NK cells, we first analyzed the receptor profile of NK cells cultured in media containing IL-15 alone or IL-15 supplemented with NAM. Flow

[1]Division of Hematology, Oncology and Transplantation, Department of Medicine, University of Minnesota, Minneapolis, MN 55455, USA. [2]University of Minnesota Institute for Health Informatics, University of Minnesota, Minneapolis, MN 55455, USA. [3]Center for Cellular Immunotherapies, Perelman School of Medicine at the University of Pennsylvania, Philadelphia, PA 19104, USA. [4]Department of Pathology and Laboratory Medicine, Perelman School of Medicine at the University of Pennsylvania, Philadelphia, PA 19104, USA. [5]Gamida Cell, Jerusalem 91340, Israel. [6]Department of Laboratory Medicine and Pathology, University of Minnesota, Minneapolis, MN 55455, USA. [7]Biostatistics Core, Masonic Cancer Center, University of Minnesota, Minneapolis, MN 55455, USA. [8]Division of Radiology, Department of Medicine, University of Minnesota, Minneapolis, MN 55455, USA. [9]Metabolic Disease Research and Thrombosis Research Center, Departments of Cardiovascular Sciences, Temple University Lewis Katz School of Medicine, Philadelphia, PA 19104, USA.
*Corresponding author. Email: cich0040@umn.edu (F.C.); bach0173@umn.edu (V.B.)
†Present address: Simcere Innovation Inc., Cambridge, MA 02142, USA.
‡Present address: Department of Medicine, City of Hope, Duarte, CA 91010, USA.

cytometry was used to assess inhibitory receptors [inhibitory killer cell immunoglobulin–like receptor (KIR) and NKG2A], activating receptors (CD2, CD16, NKp30, NKp46, and 2B4), the terminal differentiation antigen CD57, and adhesion/homing receptors [lymphocyte function–associated antigen 1 (LFA-1), CD62L, and CD44]. No differences in the frequencies of cells expressing activating receptors, inhibitory receptors, or CD57 were observed. However, CD62L and CD44 were considerably higher on the surface of NK cells cultured with IL-15 and NAM (Fig. 1A).

CD62L has been studied extensively in T cells and regulates the entry of naïve and central memory T cells into lymph nodes and sites of viral infection (*6*). CD44 binds hyaluronate on the surface of endothelial cells and enables adhesion, which is required for lymphocyte extravasation to inflammatory sites (*7*). To further substantiate our findings, NK cells from 16 additional donors were cultured under the same conditions and analyzed by flow cytometry. This analysis confirmed increases in the frequency and density of CD62L on NK cells cultured with IL-15 and NAM (Fig. 1B). In an analysis of NK cells from five more donors, we observed higher surface density of CD44 with the addition of NAM (Fig. 1C). Because CD62L was the most dynamically regulated receptor in our analyses, we decided to focus on how NAM regulates CD62L.

To determine whether NAM prevents cytokine-induced loss of CD62L or promotes de novo induction, $CD56^{bright}$, $CD56^{dim}CD62L^{+}$, and $CD56^{dim}CD62L^{-}$ NK cell subsets were sorted and cultured for 14 days with IL-15 ± NAM. $CD56^{bright}$ NK cells cultured with IL-15 alone down-regulated CD62L at days 7 and 14. In contrast, most $CD56^{bright}$ NK cells cultured with IL-15 and NAM maintained surface CD62L. Similar trends were observed for $CD56^{dim}CD62L^{+}$ NK cells. $CD56^{dim}CD62L^{-}$ NK cells cultured with IL-15 and NAM displayed a modest elevation of CD62L after 7 days of culture and much greater induction after 14 days (Fig. 2A). NAM did not markedly affect the expansion in cultures with bulk NK cells (fig. S1A) and sorted NK cell subsets (fig. S1B).

To test the stability of CD62L induction, NK cells were cultured as described above and injected intraperitoneally into NOD.Cg-*Prkdc*^{scid}/J (NSG) mice. Mice were sacrificed on days 7 and 14, and NK cells were harvested for flow cytometry analysis (Fig. 2B). NK cells cultured with IL-15 and NAM maintained high CD62L through day 14 compared with NK cells cultured with IL-15 alone (Fig. 2C). To investigate whether NAM stabilized CD62L on the surface of NK cells by preventing activation-induced cleavage, NK cells were cultured overnight with IL-12 and IL-18 with or without NAM and BMS566394, which is a small-molecule inhibitor of ADAM17, a metalloproteinase that cleaves both CD62L and CD16 (*8*, *9*). Both CD62L and CD16 were cleaved from the surface of NK cells in response to short-term cytokine stimulation regardless of NAM supplementation. This clipping was efficiently blocked with BMS566394 treatment (fig. S2). Thus, NAM prevented cytokine-induced loss of CD62L in a metalloprotease-independent fashion and promoted the induction of CD62L. Furthermore, elevated CD62L was stable in vivo after NAM withdrawal.

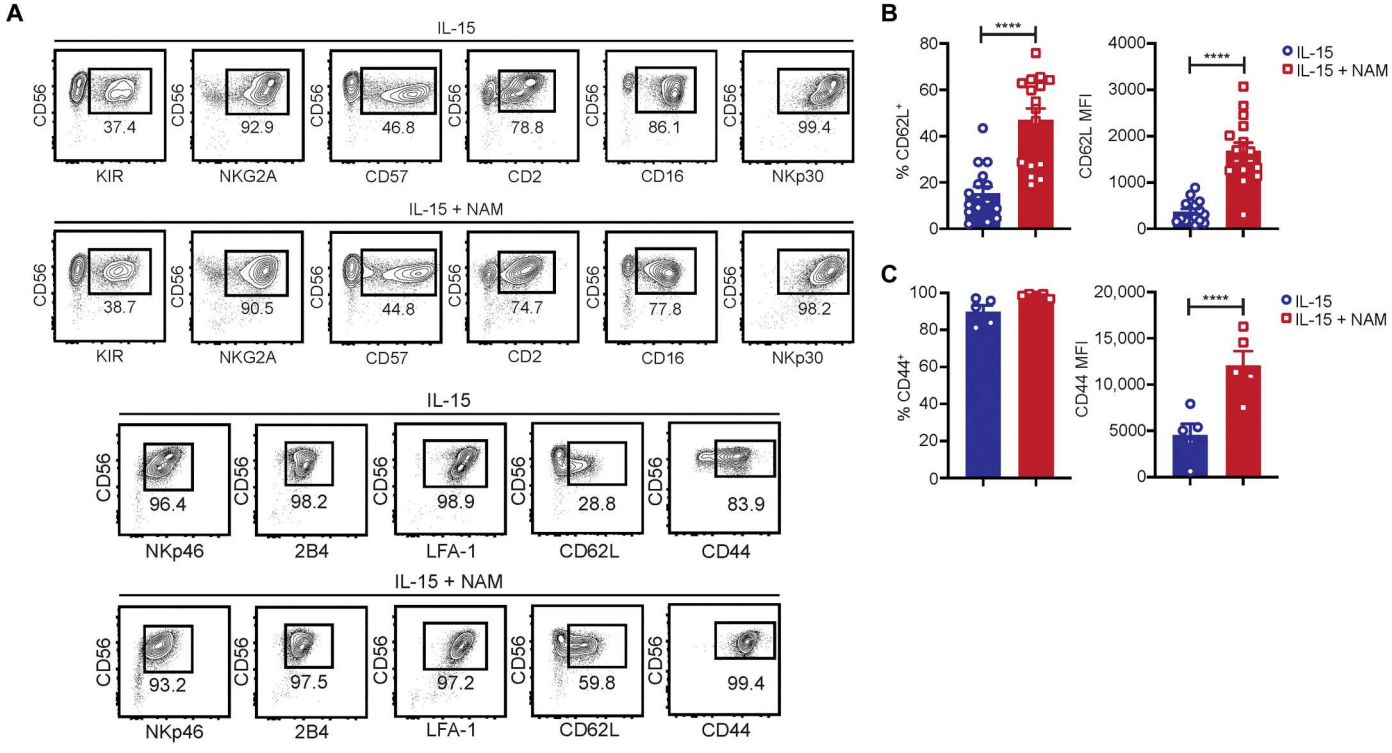

Fig. 1. NK cells cultured ex vivo with NAM display elevated CD62L and CD44. (**A**) CD3/CD19-depleted PBMCs were cultured for 14 days with IL-15 ± NAM and analyzed by flow cytometry. Representative flow cytometry plots of the indicated surface antigens on NK cells cultured in each condition are shown. Data are representative of two independent experiments. The frequency and density of CD62L (**B**) ($n = 16$) and (**C**) CD44 ($n = 5$) on NK cells cultured ex vivo with IL-15 ± NAM. Statistical significance was determined using Student's *t* tests. ****$P \leq 0.0001$. MFI, mean fluorescence intensity.

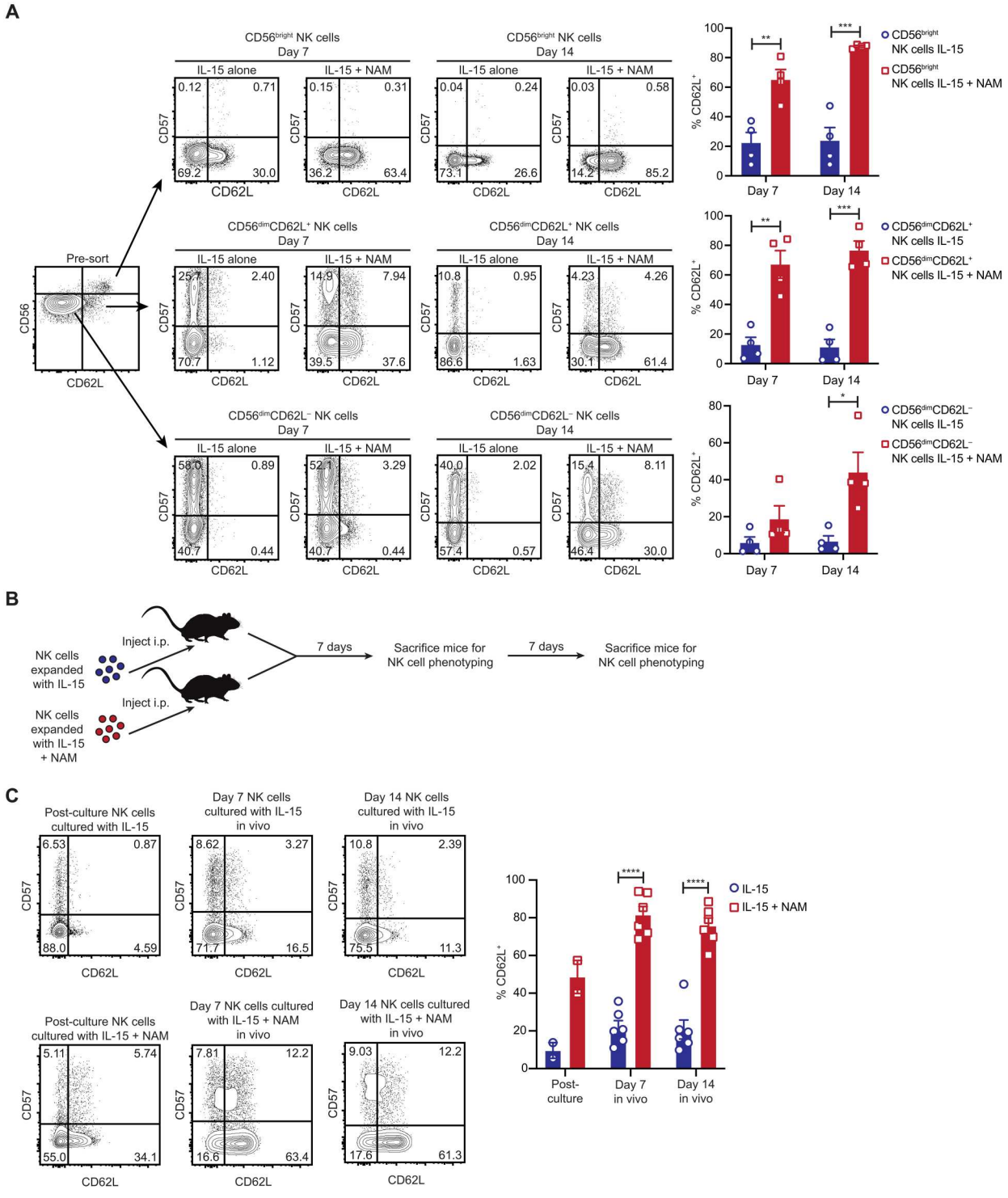

Fig. 2. NAM promotes stable cell surface CD62L. (**A**) The indicated NK cell subsets were sorted and cultured for 14 days with IL-15 ± NAM. Left: Flow cytometry plots of CD62L and CD57 at days 7 and 14 from a representative donor. Right: Cumulative data from four independent experiments. (**B**) Experimental design for xenogeneic adoptive transfer experiments testing the stability of CD62L after NAM withdrawal. CD3/CD19-depleted PBMCs were cultured for 14 days with IL-15 ± NAM and then injected intraperitoneally (i.p.) into NSG mice. Groups of mice were sacrificed at days 7 and 14. The peritonea of mice were washed, and cells were collected for analysis of CD62L on human NK cells by flow cytometry. (**C**) Left: Flow cytometry plots of CD62L and CD57 on NK cells from each culture condition on days 7 and 14 after adoptive transfer from a representative donor. Right: Cumulative data from six donors in two independent experiments. Statistical significance was determined using Student's *t* tests. *$P \leq 0.05$, **$P \leq 0.01$, ***$P \leq 0.001$, and ****$P \leq 0.0001$.

NAM prevents *FOXO1* degradation, allowing for enhanced transcription of *SELL*

In mice, forkhead box O1 (*Foxo1*) deficiency impairs peripheral T cell homeostasis and is associated with reduced CD62L protein and *Sell* (the gene encoding CD62L) mRNA (*10*). Mouse NK cells with *Foxo1* deletion also exhibit homing deficiencies and reduced surface CD62L (*11*). Considering these previous studies, we hypothesized that NAM increases FOXO1 in NK cells for elevated transcription of *SELL*. To test this, NK cells cultured with IL-15 ± NAM were analyzed by quantitative reverse transcription polymerase chain reaction (qRT-PCR) for expression of *FOXO1* and *SELL*. Whereas *SELL* mRNA was about fourfold higher in NK cells cultured with NAM, *FOXO1* mRNA expression was unaltered (Fig. 3A). We next analyzed FOXO1 protein in these cells and observed an about twofold increase in FOXO1 protein in NK cells cultured with NAM (Fig. 3B). This finding was confirmed by confocal microscopy. FOXO1 was predominantly seen in the nuclei (Fig. 3C).

Because NAM increased FOXO1 protein but did not affect *FOXO1* mRNA, we sought to determine whether NAM promotes FOXO1 stabilization. NK cells were cultured overnight with IL-15 ± NAM and then treated with cycloheximide to inhibit protein synthesis. In NK cells cultured with IL-15 alone, FOXO dropped markedly after 3 hours of treatment. By contrast, FOXO1 was maintained in NK cells cultured with IL-15 and NAM, suggesting a stabilizing effect (Fig. 3D). To determine whether NAM influences FOXO1 ubiquitination and proteasomal degradation, NK cells were again cultured overnight with IL-15 ± NAM and then incubated with or without the proteasome inhibitor MG132. Cell lysates were used in coimmunoprecipitation assays where FOXO1 was immunoprecipitated and blotted with an antibody against ubiquitin. In the absence of MG132, cells cultured with NAM exhibited less ubiquitinated FOXO1 relative to cells cultured with IL-15 alone. After treatment with MG132, ubiquitinated FOXO1 increased in cells from both culture conditions but to a greater extent in NK cells cultured with IL-15 alone (Fig. 3E).

Phosphorylation of FOXO transcription factors at three conserved sites (Tyr^{24}, Ser^{256}, and Ser^{319}) by the kinase Akt drives their export from the nucleus and subsequent degradation (*12*). To determine whether NAM could affect Akt signaling, NK cells were cultured overnight in media alone or in media supplemented with NAM. We then performed a time course stimulation with IL-15 and assessed Akt phosphorylation by Western blot. NK cells that were cultured in media alone exhibited increased phosphorylated Akt (pAkt) over time. In contrast, NK cells cultured with NAM showed diminished Akt phosphorylation in response to IL-15 stimulation (Fig. 3F). To further verify these results, peripheral blood mononuclear cells (PBMCs) were incubated overnight with or without NAM. The next day, we performed a time course stimulation assay with IL-15 and assessed pSTAT5 (phosphorylated signal transducer and activator of transcription 5) and pAkt in NK cells by intracellular flow cytometry. NK cells incubated with and without NAM exhibited similar STAT5 phosphorylation kinetics after IL-15 stimulation. However, Akt phosphorylation was higher in NK cells cultured without NAM (Fig. 3G). Next, we assessed the correlation between phosphorylated FOXO1 and CD62L. We again sorted $CD56^{bright}$, $CD56^{dim}CD62L^{+}$, and $CD56^{dim}CD62L^{-}$ NK cells and cultured each subset for 14 days with IL-15 ± NAM. FOXO1 phosphorylation was assessed by flow cytometry using an antibody specific for phosphorylation at the Ser^{256} residue. For all NK cell subsets, the $CD62L^{+}$ population displayed less phosphorylated FOXO1 relative to the $CD62L^{-}$ population (fig. S3).

To directly test the hypothesis that NAM increases CD62L through FOXO1, NK cells were cultured with IL-15 ± NAM ± AS1842856, a small-molecule inhibitor that blocks the transcriptional activity of FOXO1. NAM increased the frequency of CD62L on the cell surface. However, CD62L frequencies were reduced on NK cells cultured with AS1842856 regardless of NAM supplementation (Fig. 3H). In addition, we performed chromatin immunoprecipitation (ChIP) assays to assess FOXO1 binding to the proximal promoter of *SELL*. In human cells, FOXO1 binds to a conserved CCCTTTGG motif within the proximal promoter (*13*). We observed marked enrichment of FOXO1 binding to this site in NK cells cultured with NAM (Fig. 3I). Together, these data showed that NAM promotes FOXO1 protein stabilization, allowing for enhanced *SELL* transcription.

NK cells cultured with NAM have unique metabolic attributes and are protected against oxidative stress

NAM supplementation improves aspects of health span in mice (*14*). How NAM affects immune cell metabolism has not been thoroughly assessed. Using colorimetric assays, we found that the concentrations of NAD^{+} [nicotinamide adenine dinucleotide (oxidized form)], NADH (reduced form of NAD^{+}), $NADP^{+}$ (nicotinamide adenine dinucleotide phosphate), NADPH (reduced form of $NADP^{+}$), and ATP (adenosine 5′-triphosphate) were elevated in NK cells cultured with NAM (Fig. 4A). NAD^{+}/NADH and $NADP^{+}$/NADPH redox couples serve as cofactors for numerous enzymes to retain cellular redox balance and energy metabolism (*15*). To gain a deeper understanding of the metabolic effects associated with NAM, we performed a comprehensive evaluation of principle metabolites using mass spectrometry. Consistent with the colorimetric assays, large increases in NAM, nicotinate, and NAD^{+} were seen in NK cells cultured with NAM. We also observed elevations of metabolites involved in polyamine metabolism. Polyamines are essential for cell growth and proliferation. They stabilize DNA and RNA and have antioxidant activities (*16*). NK cells cultured with NAM also exhibited increased glutathione, glutamate, glycine, and threonine. Glutathione is particularly important, because it plays a central role in redox reactions that neutralize reactive oxygen species (ROS) (*17*). Additional metabolic pathways influenced by NAM included the tricarboxylic acid (TCA) cycle, the pentose phosphate pathway (PPP), and glycolysis (table S1) (Fig. 4B).

Because NK cells cultured with NAM exhibited higher NADPH and glutathione, we wanted to determine whether NAM supplementation could protect NK cells from oxidative stress. NK cells were cultured overnight with IL-15 ± NAM and then incubated with hydrogen peroxide (H_2O_2). Cells were then stained with MitoSOX dye for detection of mitochondrial superoxide by flow cytometry. NK cells cultured with IL-15 and NAM displayed markedly less mitochondrial superoxide relative to NK cells cultured with IL-15 alone (Fig. 4C). Elevations of several metabolites within the glycolysis and TCA cycle pathways in NK cells expanded with NAM (Fig. 4B) were suggestive of increased glucose flux. To confirm this, NK cells were cultured for 14 days with IL-15 ± NAM. Cells were then washed and placed in media containing $^{13}C_6$ glucose for carbon tracing. We observed an about threefold increase in labeled acetyl–coenzyme A (acetyl-CoA) by liquid

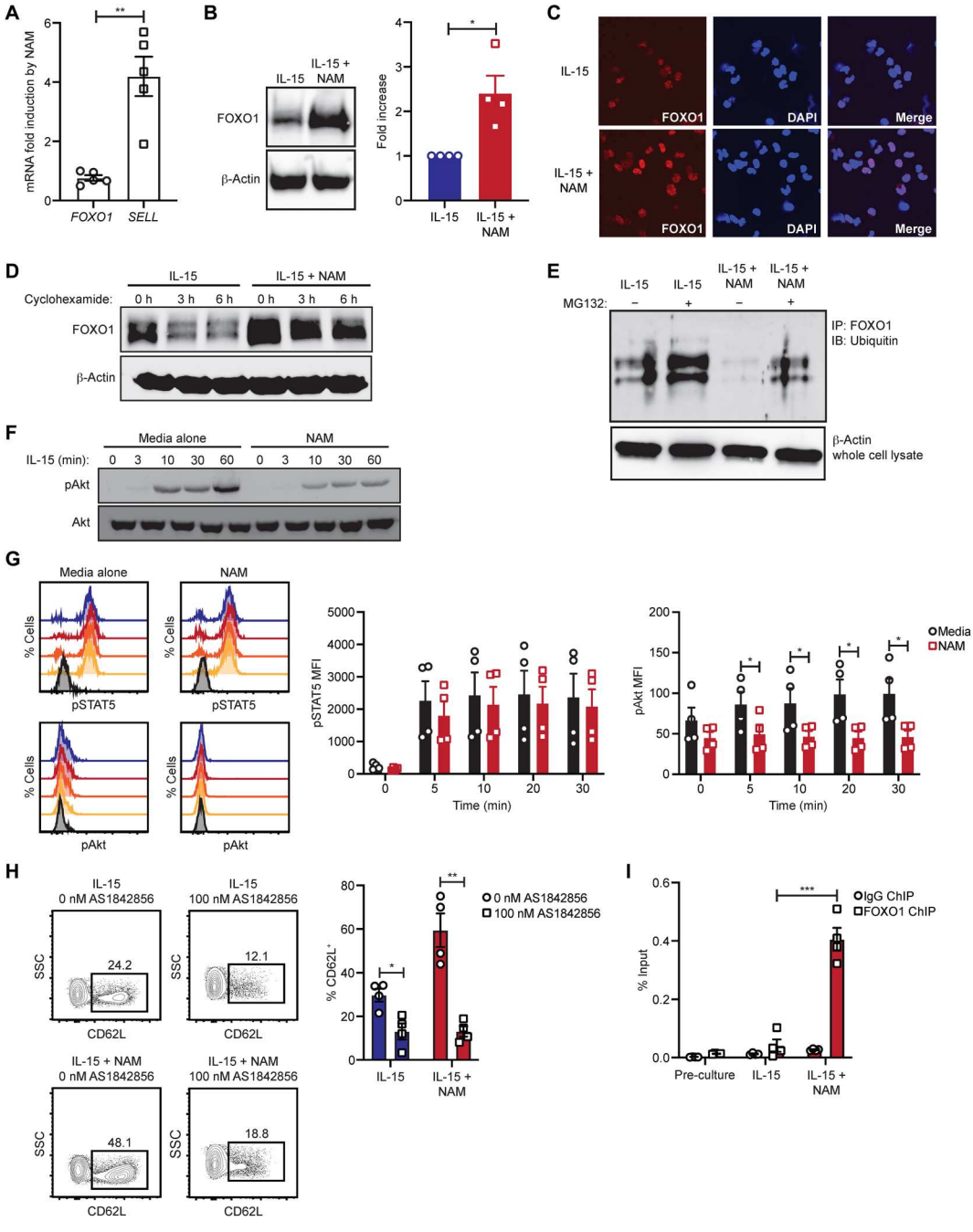

Fig. 3. NAM prevents FOXO1 degradation for enhanced *SELL* expression. (**A**) CD3/CD19-depleted PBMCs were cultured for 14 days with IL-15 ± NAM. *FOXO1* and *SELL* mRNA were determined by quantitative real-time PCR ($n = 5$) in two independent experiments. All data were normalized against *ACTB*. (**B**) FOXO1 protein was assessed by Western blot. FOXO1 and β-actin blots from a representative donor (left) and cumulative data of the relative FOXO1 fold increases in NK cells cultured with NAM (right) are shown. Data are from four donors in two independent experiments. (**C**) FOXO1 protein (red) was analyzed by confocal microscopy. Nuclei are stained blue. Images are representative of two donors analyzed. (**D**) NK cells were isolated and cultured overnight with IL-15 ± NAM. The next day, cells were cultured for 0, 3, and 6 hours with cycloheximide (10 mg/ml). FOXO1 protein was determined by Western blot. Data from a representative experiment ($n = 2$) are shown. (**E**) NK cells were cultured overnight with IL-15 ± NAM. The next day, cells were cultured in the absence or presence of 10 mM MG132 for 6 hours. FOXO1 ubiquitination was assessed by coimmunoprecipitation. Data are representative of two independent experiments. (**F**) NK cells were cultured for 0, 3, 10, 30, or 60 min with IL-15. Cells were fixed and lysed at each time point for assessment of total and phosphorylated Akt. Data are representative of two independent experiments. (**G**) PBMCs were isolated and rested overnight in the absence of exogenous cytokines ± NAM. The next day, cells were cultured for 0, 5, 10, 20, or 30 min with IL-15. Phosphorylated STAT5 and Akt were analyzed by intracellular flow cytometry. Flow cytometry histogram plots from a representative donor (left) and cumulative data from four donors in two independent experiments (right) are shown. (**H**) NK cells were cultured for 14 days with IL-15 ± NAM ± 100 nM AS1842856. Flow cytometry plots of CD62L on NK cells from a representative donor (left) and cumulative data from four donors in two independent experiments (right) are shown. SSC, side scatter. (**I**) NK cells were cultured as described in (A). Lysates from these cells were used in ChIP assays to assess FOXO1 binding to the *SELL* promoter. All data were normalized to input. Statistical significance was determined using Student's *t* tests. $*P \leq 0.05$ and $**P \leq 0.01$.

chromatography–mass spectrometry analysis in NK cells cultured with NAM compared with NK cells cultured with IL-15 alone (Fig. 4D), demonstrative of heightened glucose flux. To assess overall metabolic activity, we performed real-time metabolic flux assays to measure readouts of glycolysis and mitochondrial oxidative phosphorylation. We observed higher glycolytic capacity and glycolytic reserve, ATP-linked respiration, and maximal respiration in NK cells cultured with NAM (Fig. 4E). Together, these data showed that NAM alters NK cell metabolism for enhanced protection against oxidative stress and increased glucose flux through the TCA cycle.

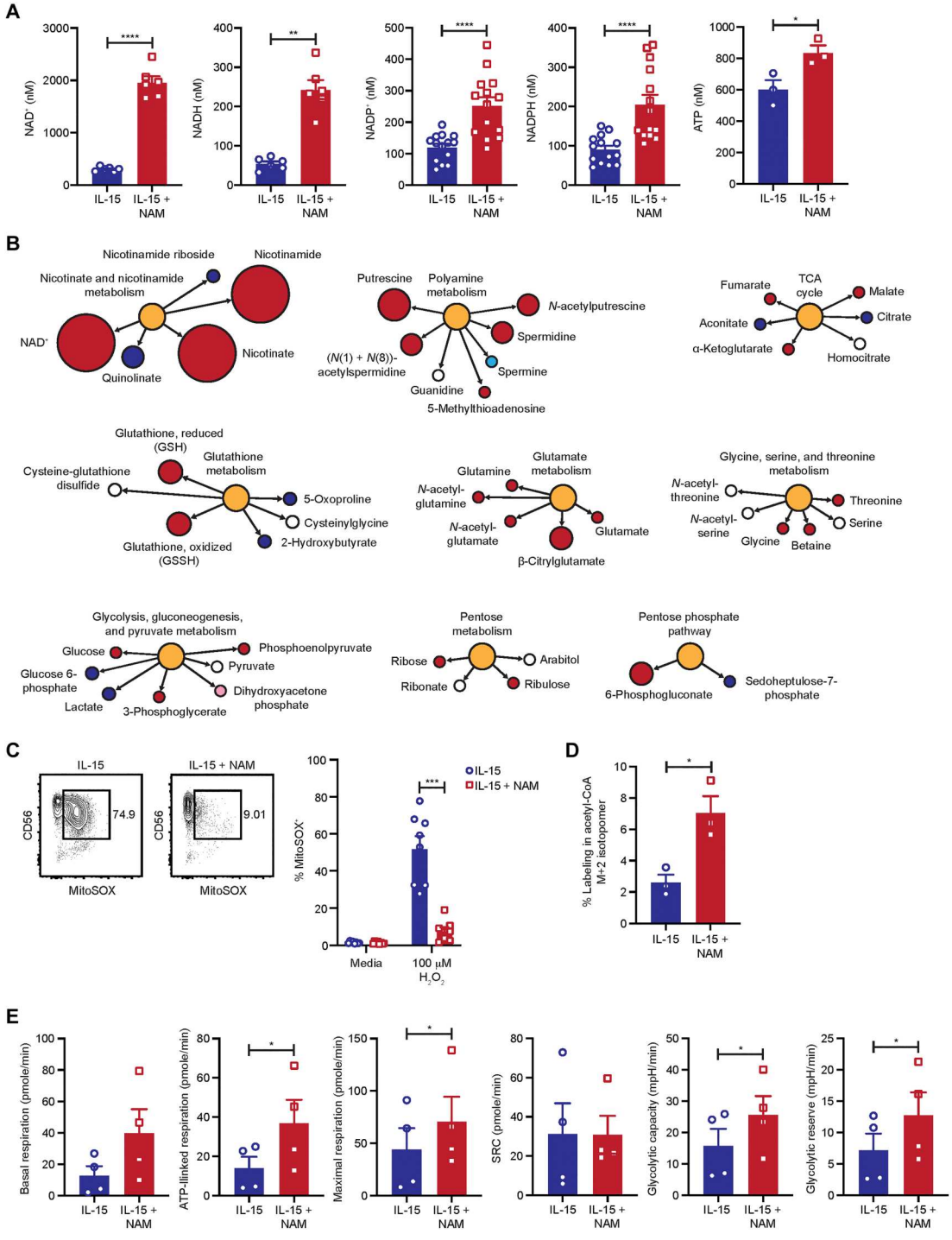

Fig. 4. NAM affects multiple metabolic pathways and promotes NK cell resistance to oxidative stress. (**A**) NK cells were cultured for 14 days with IL-15 ± NAM. Colorimetric assays were used to measure NAD^+ ($n = 6$), NADH ($n = 6$), $NADP^+$ ($n = 14$), NADPH ($n = 14$), and ATP ($n = 3$). (**B**) NK cells from 24 donors were cultured as described in (A), and global metabolic profiles were determined by mass spectrometry. Metabolic pathways that were altered by NAM supplementation are shown. Red indicates metabolites that were significantly higher in NK cells cultured with IL-15 and NAM, blue indicates metabolites that were significantly higher in NK cells cultured with IL-15 alone, and white indicates no statistically significant difference between groups. Light red and blue circles represent metabolites that approached statistical significance. The size of the circles reflects the magnitude of the difference. (**C**) NK cells were cultured as described in (A) and incubated with or without 100 mM H_2O_2 for 1 hour. Cells were then stained with MitoSOX dye and analyzed by flow cytometry. Representative flow cytometry plots (left) and cumulative data from eight donors in four independent experiments (right) are shown. (**D**) Enriched NK cells from three donors were cultured for 14 days with IL-15 ± NAM. Cells were then washed and put into media containing $^{13}C_6$ glucose. Analysis of carbon-labeled acetyl-CoA was performed by mass spectrometry. (**E**) Real-time metabolic profiling of NK cells cultured for 14 days with IL-15 ± NAM was performed by Seahorse. Cumulative data from four donors in two independent experiments are shown. Statistical significance was determined using Student's *t* tests. *$P \leq 0.05$, **$P \leq 0.01$, ***$P \leq 0.001$, and ****$P \leq 0.0001$.

NK cells cultured with NAM exhibit enhanced antitumor function and in vivo persistence

We next sought to evaluate the effect of NAM on NK cell function. We cultured NK cells with IL-15 ± NAM and then set up cocultures with K562 cells. NK cells cultured with NAM exhibited higher frequencies of degranulation (as indicated by surface CD107 staining), tumor necrosis factor (TNF) production, and IFN-γ production (Fig. 5A). To directly assess cytotoxicity, we performed live imaging IncuCyte assays using K562 cells transduced with NucLight Red at effector:target (E:T) ratios ranging from 0.5:1 to 2:1. At each E:T ratio, NK cells cultured with IL-15 and NAM displayed more rapid killing kinetics (Fig. 5B). To assess the effect of NAM on individual NK cell subsets, we sorted CD56^{bright}, CD56^{dim}CD62L^{+}, and CD56^{dim}CD62L^{-} NK cells and cultured them as described above. These cells were used as effectors against NucLight Red–expressing K562 cells. Although NAM did not substantially increase the cytotoxicity of CD56^{dim}CD62L^{-} NK cells, CD56^{bright} and CD56^{dim}CD62L^{+} NK cell–killing kinetics were enhanced by NAM (Fig. 5C). To evaluate antibody-dependent cellular cytotoxicity (ADCC), NK cells cultured with IL-15 ± NAM were cocultured

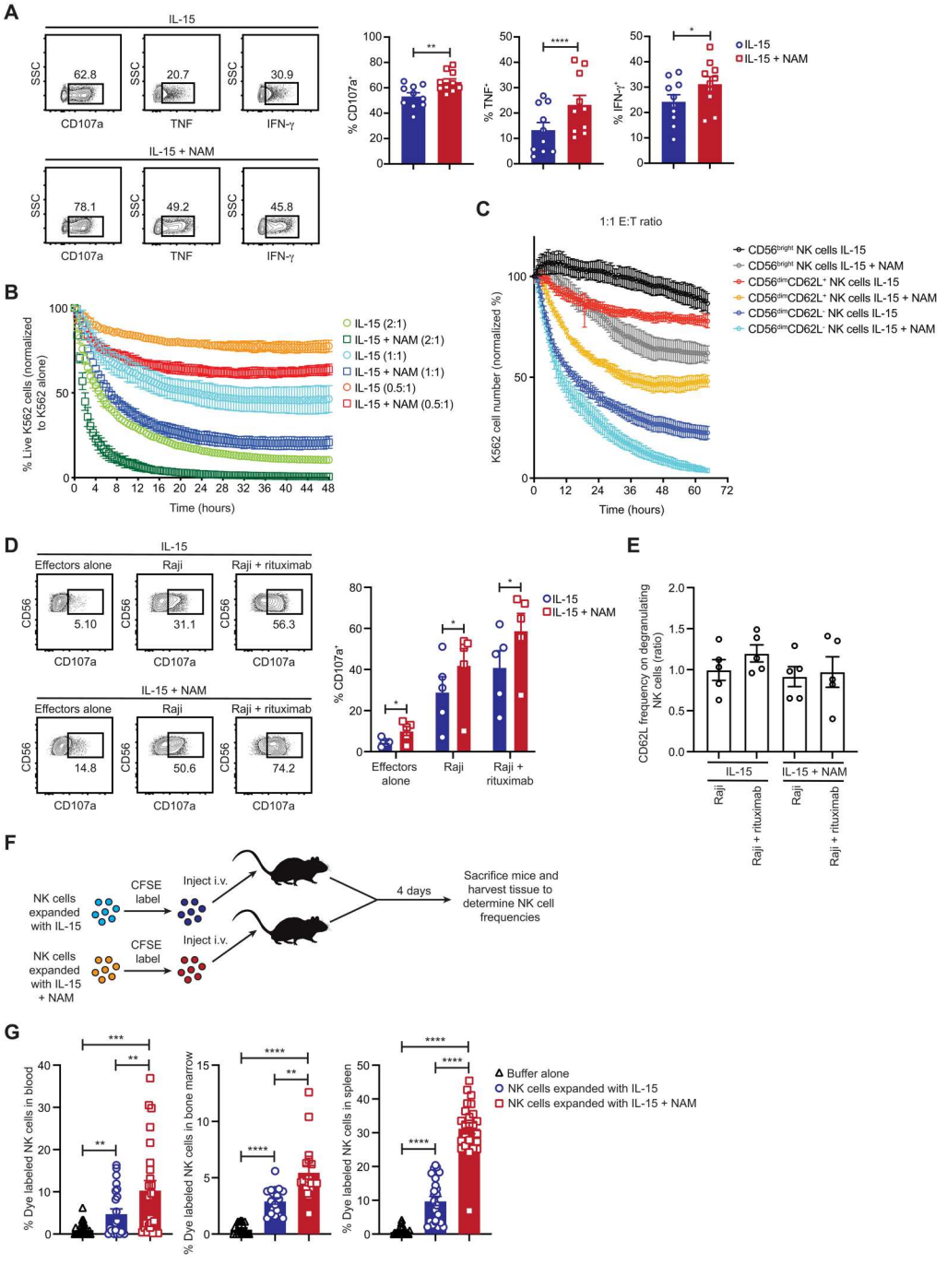

Fig. 5. NAM enhances NK cell function and tissue retention. (**A**) NK cells from 10 donors were cultured for 14 days with IL-15 ± NAM. NK cells were then cocultured with K562 cells at a 2:1 E:T ratio for 5 hours. NK cell degranulation, TNF production, and IFN-γ production were assessed by flow cytometry. Flow cytometry plots from a representative experiment (left) and cumulative data from four independent experiments (right) are shown. (**B**) Enriched NK cells and (**C**) sorted NK cell subsets were cultured as described above and then cocultured with K562 cells transduced with NucLight Red at the indicated E:T ratios. Cytotoxicity was assessed in real time by IncuCyte imaging. Data are representative of two independent experiments. Statistical significance was determined using Student's *t* tests. (**D**) Enriched NK cells from five donors were cultured for 7 days with IL-15 ± NAM. NK cells were then cocultured with Raji cells alone or with rituximab (1 μg/ml) at a 2:1 E:T ratio and analyzed by flow cytometry. Frequencies of surface CD107a on NK cells from each condition for a representative donor (left) and cumulative graphed data (right) are shown. Statistical significance was determined using Student's *t* tests. (**E**) Ratios of CD62L frequencies on the surface of CD107a^{+} and CD107a^{-} NK cells in the functional assay using Raji targets with and without rituximab for each culture condition. (**F**) Schematic illustrating the experimental design to assess NK cell frequencies in tissues after adoptive transfer. NK cells from five donors were cultured for 14 days with IL-15 ± NAM and labeled with CFSE dye. Cells (1.5×10^7) were injected intravenously into each mouse. Control mice received injections of human serum albumin (HSA) buffer alone. Mice were sacrificed after 4 days, and blood, bone marrow, and spleen tissues were harvested. The frequencies of dye-labeled human NK cells were determined by flow cytometry. (**G**) Cumulative data from five independent experiments performed with 6 mice per group for a total of 90 mice. Statistical significance was determined by one-way ANOVA. *$P \leq 0.05$, **$P \leq 0.01$, ***$P \leq 0.001$, and ****$P \leq 0.0001$.

with Raji cells in the absence or presence of rituximab. Both natural cytotoxicity and ADCC were markedly higher for NK cells cultured with NAM (Fig. 5D). CD62L was generally maintained on degranulating cells in these assays (Fig. 5E). Supplementation of NAM during cord blood–derived NK cell and induced pluripotent stem cell–derived NK cell culture did not affect degranulation or CD62L (fig. S4), suggesting that plasticity and heterogeneity within the adult peripheral blood NK cell population may be important for the effects of NAM. Similarly, NAM supplementation enhanced canonical but not NKG2C$^+$ adaptive NK cell degranulation in response to Raji cells with and without rituximab (fig. S5). Because adaptive NK cells exhibit elevated metabolic activity relative to canonical NK cells ex vivo (*18*), this specialized subset may be less affected by NAM supplementation.

Next, we assessed the distribution of cells in vivo after adoptive transfer. NK cells were cultured with IL-15 ± NAM, labeled with carboxyfluorescein diacetate succinimidyl ester (CFSE) dye, and infused into NSG mice. Mice were sacrificed 4 days after cell transfer, and blood, bone marrow, and spleen tissues were collected to determine the frequencies of CFSE-labeled cells (Fig. 5F). For each tissue analyzed, we observed higher frequencies of NK cells that were cultured with NAM (Fig. 5G). Together, these data demonstrated positive effects of NAM on enhancing NK cell antitumor function and in vivo persistence.

CRs were observed after NAM-expanded NK cell infusion in patients with R/R NHL

On the basis of our preclinical findings, we initiated a first-in-human phase 1 clinical trial of adoptive transfer of human leukocyte antigen (HLA)–haploidentical donor-derived NAM-expanded allogeneic NK cells (GDA-201) processed in a good manufacturing practices (GMP) facility for the treatment of patients with R/R NHL and multiple myeloma (MM) (NCT03019666) (Fig. 6A). The protocol synopsis and NK cell isolation and expansion information are included in the Supplementary Materials. In this study, patients received three doses of rituximab (NHL) or elotuzumab (MM) and lymphodepleting chemotherapy followed by GDA-201 and low-dose IL-2 (Fig. 6B). Patient demographics are shown in table S2. A total of 39 patients were enrolled, and 20 had NHL. Nine patients had diffuse large B cell lymphoma (DLBCL), 10 had follicular lymphoma (FL), and 1 had mantle cell lymphoma. Patients were treated at three dose cohorts: 2×10^7, 1×10^8, or 2×10^8 GDA-201 cells/kg. GDA-201 therapy was well tolerated, and most adverse events were grades 1 and 2 and included chills, IL-2 injection site reactions, fatigue, and nausea. The most common grade 3 and 4 adverse events were thrombocytopenia ($n = 4$), febrile neutropenia ($n = 4$), and anemia ($n = 3$). There was no evidence of CRS, neurotoxicity, GvHD, or marrow aplasia. A complete summary of adverse events is included as table S3, and final GDA-201 product characteristics are included as table S4. One patient died of *Escherichia coli* sepsis.

Among 19 patients with NHL evaluable for response, 11 (57%) had a CR, and 3 patients had a partial response (PR) for an overall response (OR) rate of 74%. All patients exhibited a clinical response within 28 days after GDA-201 infusion. Four patients with NHL received a second dose of GDA-201 without additional lymphodepleting chemotherapy. Two patients (one with FL and one with DLBCL) showed a further deepening of response from PR to CR (Fig. 6C). The median duration of response was 16 months (range, 5 to 36 months). Progression-free survival (PFS) at 1 and 2 years was estimated at 50% [95% confidence interval (CI), 27 to 69%] and 35% (95% CI, 14 to 58%), respectively (Fig. 6D). Two patients underwent allogeneic hematopoietic stem cell transplantation (HSCT), and one had autologous HSCT for consolidation. After censoring for transplant, the PFS at 2 years was 19% (95% CI, 2 to 51%), and overall survival at 2 years was 73% (95% CI, 43 to 89%) (Fig. 6E). For 15 patients, donor NK cells could be distinguished by differences in HLA haplotypes. Chimerism in the peripheral blood was determined by flow cytometry. GDA-201 cells persisted in peripheral blood up to days 7 to 14 [day 4 average = 47% (range, 4.7 to 98%; day 7 average = 19% (range, 0 to 58%)] (Fig. 6F). There was no clear correlation between donor NK cell chimerism and clinical responses. Together, these results showed that GDA-201 with rituximab was well tolerated and was associated with promising clinical activity, in vivo persistence, and trafficking to tumor-involved tissues in patients with B cell NHL. Patients with R/R MM treated with GDA-201 and elotuzumab demonstrated similar GDA-201 in vivo persistence but poor clinical responses.

We have included additional data from patient 009. This is a 57-year-old man with a history of chronic lymphocytic leukemia and Richter's transformation who progressed after multiple previous lines of therapy, including an allogeneic matched sibling HSCT. He presented with multifocal adenopathy, including large retroperitoneal lymph nodes. The patient received two cycles of GDA-201, and positron emission photography (PET) scans at 6 months after GDA-201 treatment showed a CR with continued tumor shrinkage (Fig. 7A). A lymph node core biopsy before therapy showed neoplastic large B cells (Fig. 7, B and C) and limited numbers of CD3$^+$ T cells by immunohistochemistry (Fig. 7D). A day 16 post–GDA-201 biopsy of lymph node tissue showed regressing tumor with areas of necrotic tissue with fibrosis (Fig. 7, E and F) and T cell infiltration (Fig. 7G). A dense lymphoid infiltrate consisting predominantly of T cells with occasional infiltrating NK cells was observed using co-detection by indexing (CODEX) (Fig. 7H). No evidence of residual B cells was detected (Fig. 7I), and the T cell infiltrate comprised both CD4$^+$ and CD8$^+$ subsets (Fig. 7J). We detected donor GDA-201 cells in both the blood and lymph node tissue after treatment by flow cytometry at day 14 after GDA-201 treatment (Fig. 7K), and donor NK cells exhibited superior cytotoxicity relative to host NK cells (fig. S6).

Ex vivo expansion with IL-15 and NAM drives genome-wide transcriptional changes that are maintained after adoptive transfer

Last, using samples from the clinical trial, we sought to investigate how ex vivo expansion of NK cells with IL-15 and NAM affected global transcription and whether transcriptional alterations were maintained in vivo after the GDA-201 product was adoptively transferred into patients with cancer. We sorted NK cells from three banked donor apheresis products (patients 019, 026, and 029) before and after expansion with IL-15 and NAM. We also sorted NK cells from peripheral blood samples collected 4 days after treatment using anti-HLA antibodies distinguishing between host and donor cells. All sorted populations were processed and analyzed by single-cell RNA sequencing (scRNA-seq). Apheresis NK cells, product GDA-201 NK cells, and NK cells collected from patients at day 4 separated into three distinct clusters (Fig. 8A). In a separate analysis including only day 4 GDA-201 and host NK cells,

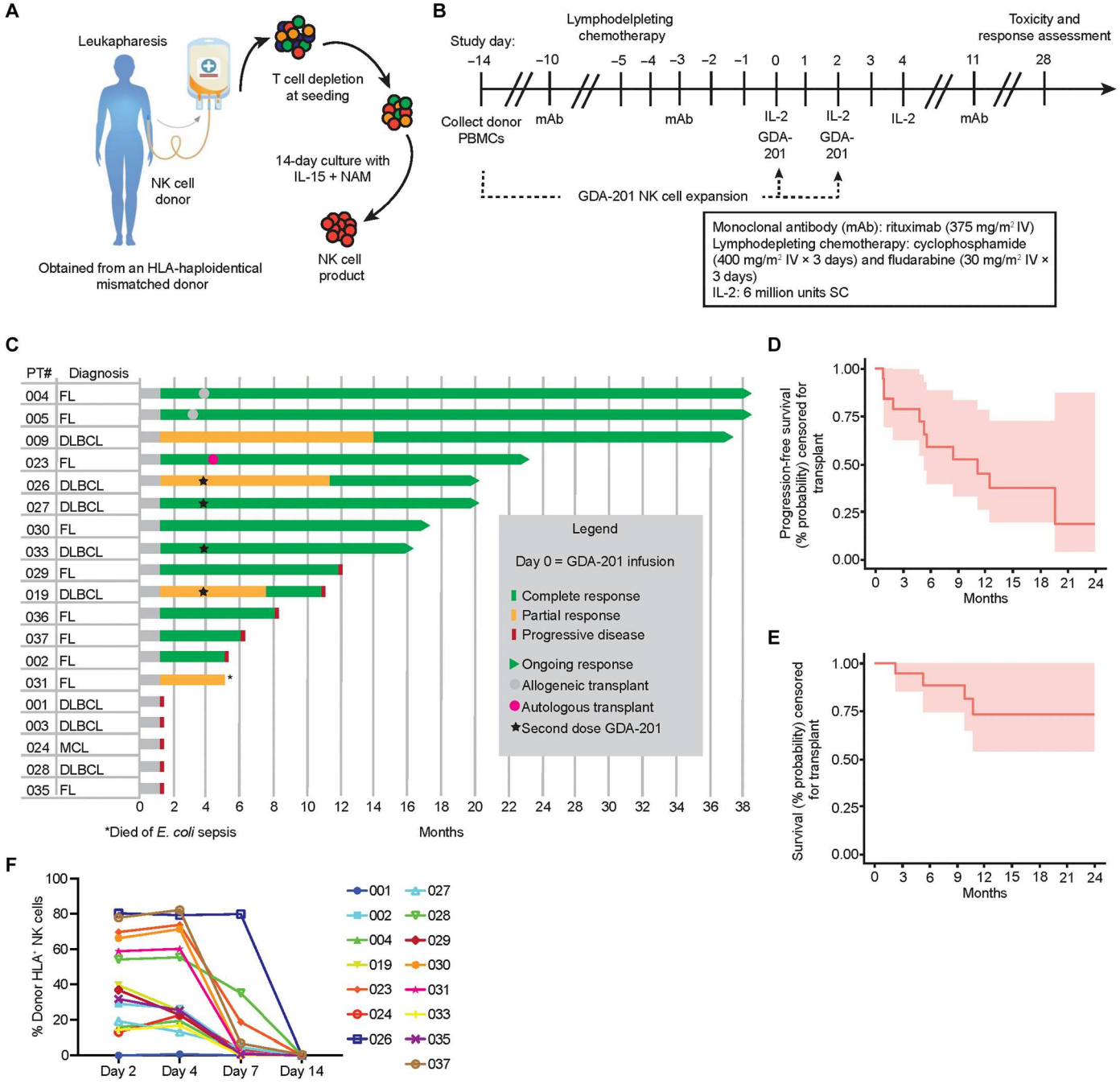

Fig. 6. Complete remissions were observed after GDA-201 treatment. (**A**) Schematic showing the steps used to generate NAM-expanded peripheral blood NK cells for immunotherapy in the GMP facility. (**B**) Schematic of the phase 1 clinical trial testing the safety and efficacy of GDA-201 in combination with monoclonal antibody (mAb) and IL-2. IV, intravenously; SC, subcutaneously. (**C**) Swimmer's plot representing disease type and duration of response for the R/R NHL cohort ($n = 19$). NHL subtype, CR or PR, ongoing response, and progressive disease are indicated. (**D**) PFS and (**E**) overall survival at 2 years for the R/R NHL cohort censored for transplant. (**F**) Percentages of donor NK cells (as a fraction of total peripheral blood NK cells) after adoptive transfer for 15 patients for whom donor and host NK cells could be distinguished using fluorescently conjugated antibodies specific for HLA-A and HLA-B alleles.

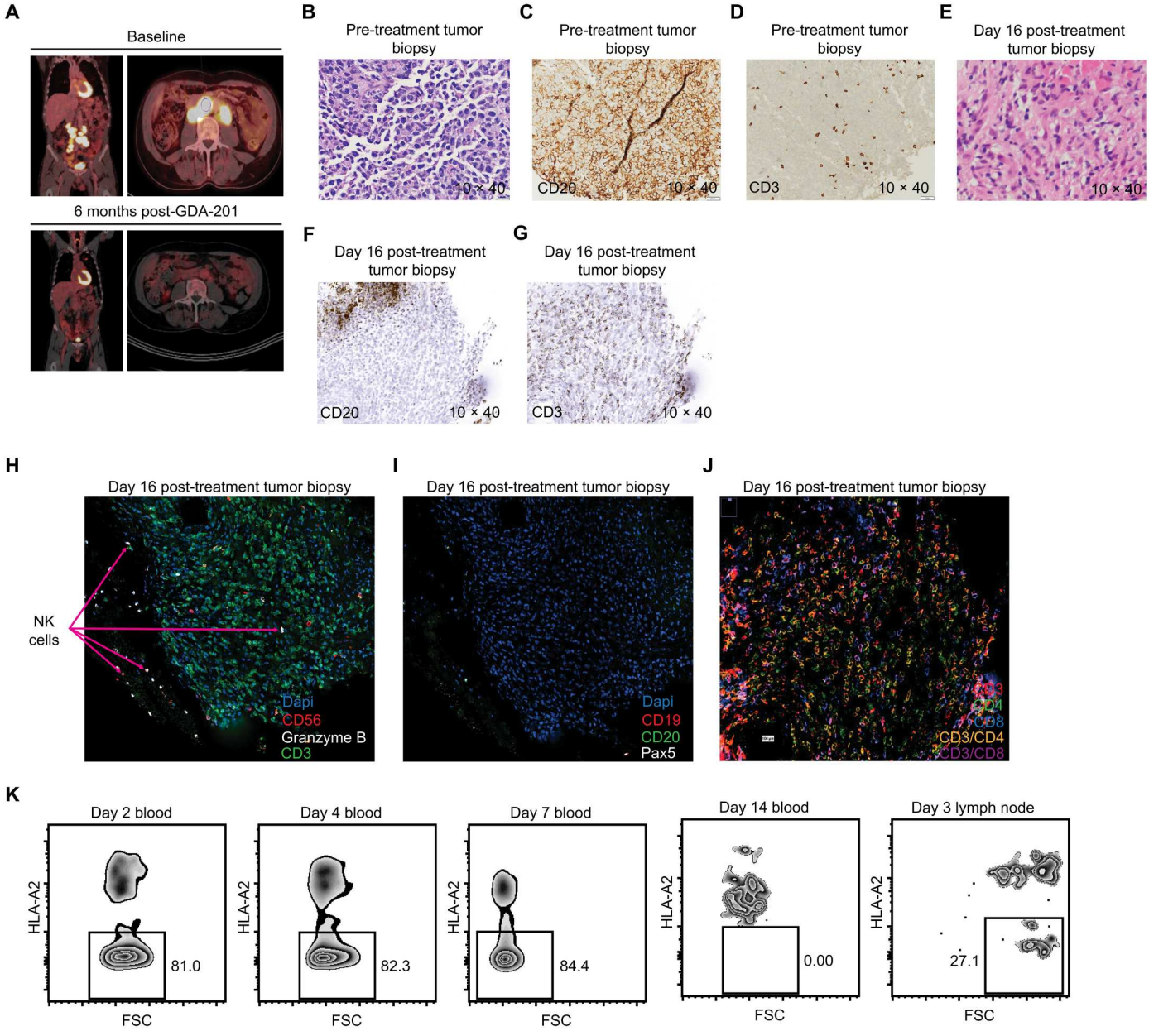

Fig. 7. Tumor regression is associated with dense host T cell infiltration into lymph node tissue after GDA-201 treatment. (**A**) PET scan of patient 009 at baseline and 6 months after GDA-201 treatment. (**B**) Hematoxylin-eosin–stained section showing histology of a lymph node core biopsy sample from patient 009 before GDA-201 treatment. (**C**) CD20 and (**D**) CD3 staining of a pretreatment lymph node biopsy sample from patient 009. (**E**) Hematoxylin-eosin–stained section showing the histology of a lymph node biopsy sample from patient 009 at day 16 after GDA-201 treatment. (**F**) CD20 and (**G**) CD3 staining of simulated immunohistochemistry derived from immunofluorescence CODEX analysis of a lymph node biopsy sample from patient 009 at day 16 after GDA-201 treatment. (**H**) CODEX-stained section showing NK and T cell infiltration within a lymph node biopsy sample from patient 009 at day 16 after GDA-201 treatment. The same section of lymph node biopsy sample was also analyzed for the presence of (**I**) B cells and (**J**) $CD4^+$ T cells and $CD8^+$ T cells. (**K**) Flow cytometry analysis of NK cells within peripheral blood and lymph node biopsy tissue at the indicated time points after GDA-201. Donor cells were detected by differences in HLA (donor NK cells are HLA-$A2^-$, and host NK cells are HLA-$A2^+$). Flow plots are gated on $CD45^+CD56^+CD3^-$ NK cells. FSC, forward scatter.

both overlapping and nonoverlapping populations were observed (Fig. 8B). In an analysis of differentially expressed transcripts between GDA-201 and apheresis NK cells and between day 4 GDA-201 and host NK cells, many of the transcripts that were elevated in GDA-201 product NK cells and day 4 GDA-201 NK cells were associated with immature $CD56^{bright}$ NK cells. Conversely, many of the transcripts that were down-regulated in GDA-201 and day 4 GDA-201 NK cells were associated with more mature $CD56^{dim}$ NK cell populations. To further illustrate these patterns, we sorted $CD56^{bright}$ NK cells, $CD56^{dim}CD94^{high}$ NK cells, and $CD56^{dim}CD94^{low/-}$ NK cells from the peripheral blood of four healthy donors and performed bulk RNA-seq. We found that,

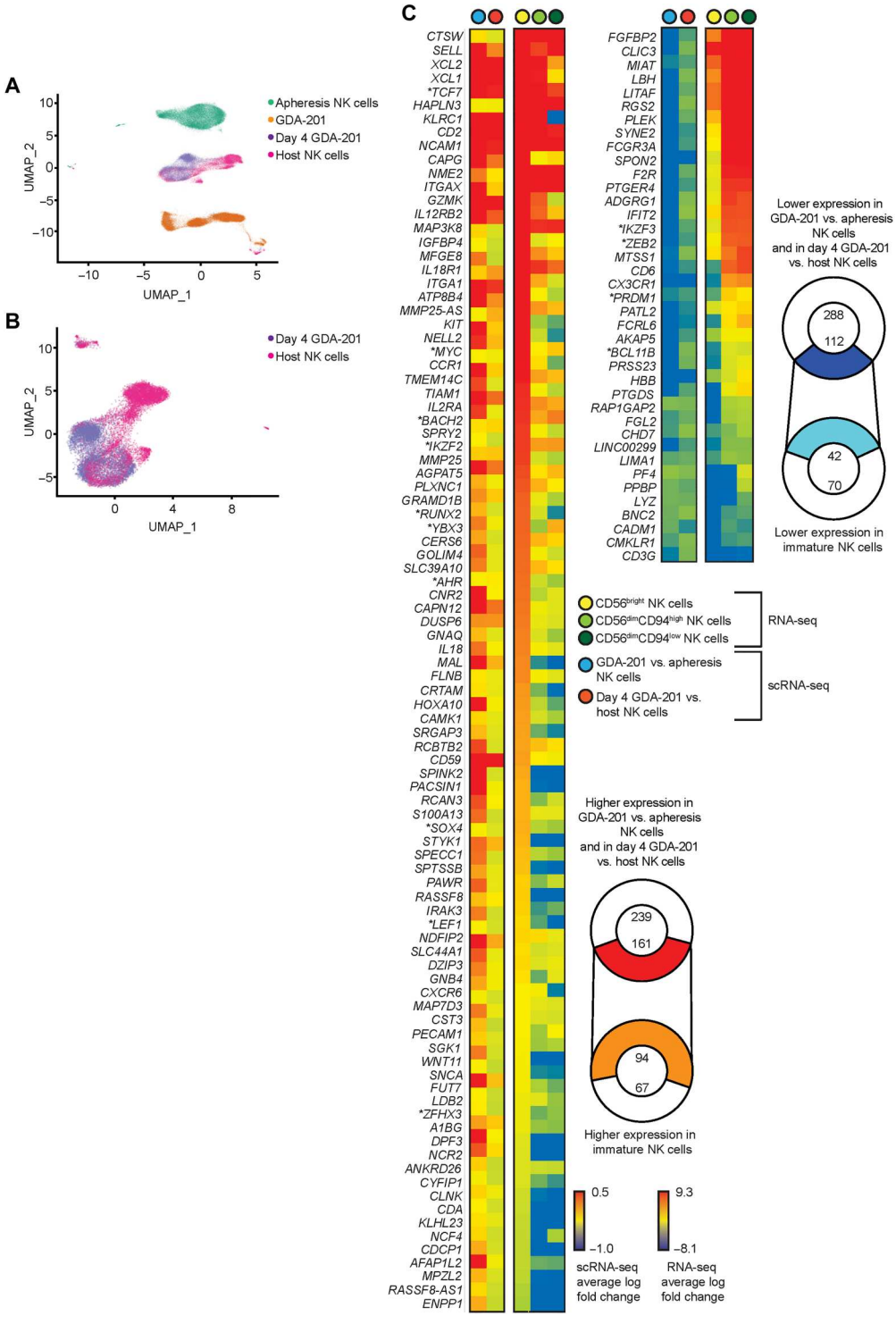

Fig. 8. NK cells expanded ex vivo with IL-15 and NAM have a transcriptional profile similar to CD56^{bright} NK cells. NK cells were sorted from banked apheresis products used to generate GDA-201 NK cells to treat three patients and from the expanded GDA-201 NK cell products. GDA-201 and host NK cells were also sorted from peripheral blood collected 4 days after treatment. All sorted populations were assessed by scRNA-seq. (**A**) Cluster analysis of all four sorted populations from three sets of product and patient samples. (**B**) Cluster analysis comparing the day 4 GDA-201 and host NK cells only. (**C**) Heatmaps of transcripts with differential expression between GDA-201 and apheresis NK cells and between day 4 GDA-201 and host NK cells. Heatmaps of relative transcript expression of the same genes in a bulk RNA-seq comparison of CD56^{bright}, CD56^{dim}CD94^{high}, and CD56^{dim}CD94$^{low/-}$ NK cells sorted from four healthy donors are also shown.

among the top 400 transcripts with higher expression in GDA-201versus apheresis NK cells, 161 were also up-regulated in the comparison between day 4 GDA-201 and host NK cells. Of these 161 transcripts, 94 had higher expression in immature CD56^{bright} NK cells. Conversely, among the top 400 transcripts with lower expression in GDA-201 versus apheresis NK cells, 112 were also down-regulated when comparing day 4 GDA-201 and host NK cells. Of these 112 transcripts, 42 had lower expression in CD56^{bright} NK cells relative to CD56^{dim} NK cells (Fig. 8C). Together, these data suggested that NK cells cultured ex vivo with IL-15 and NAM have an immature transcriptional signature that is maintained after adoptive transfer.

DISCUSSION

Here, we showed that NK cells expanded ex vivo with IL-15 and NAM had elevated NAD^+, NADH, $NADP^+$, and NADPH, which are central to redox homeostasis. Low amounts of ROS support cell proliferation and survival through posttranslational modification of phosphatases and kinases (*19*). High concentrations of ROS, however, can damage essential cellular components. Thus, maintaining redox homeostasis is critical for cell survival and function (*20*). Cells depend on multiple defense systems to maintain ROS below the toxic threshold. The glutathione and peroxiredoxin systems are maintained by NADPH, which is a universal reducing equivalent for ROS scavenging (*21*). Multiple pathways can regenerate NADPH from $NADP^+$. Among them, the oxidative PPP produces most of the NADPH in a variety of cell types (*22*). We observed higher concentrations of 6-phosphogluconate, which is the first metabolite that enters the PPP, in NK cells cultured with NAM. Elevated PPP activity, along with increases in glutathione and polyamines, in NK cells cultured with NAM may explain the profound reductions in mitochondrial ROS in response to oxidative stress.

Elevated NAD^+ in NK cells cultured with NAM may also account for their enhanced function. Recent work has shown that NAD^+ concentrations are low in tumor-infiltrating lymphocytes relative to peripheral blood T cells, and NAD^+ modulates human T cell function by regulating cellular energy metabolism. In these studies, reduced NAD^+ resulted in attenuated maximal respiratory capacity of mitochondria and concomitant decreases in adenosine 5′-diphosphate (ADP) and ATP (*23*). In agreement with this work, we observed elevated ATP and increased mitochondrial oxidative phosphorylation in NK cells cultured with NAM. These metabolic alterations correlated with enhanced natural cytotoxicity, ADCC, and inflammatory cytokine production. The elevated function of NK cells cultured with NAM could also be related to increased glycolytic metabolism. Inhibition of glycolysis has been shown to impair both mouse and human NK cell cytotoxicity after priming in vitro (*24*).

In addition to its effects on NK cell metabolism, NAM dampened Akt signaling downstream of IL-15 in NK cells cultured ex vivo. Akt can directly phosphorylate FOXO transcription factors on three sites, leading to their nuclear export and degradation (*12*). This basic mechanism is highly conserved across species (*25*). Lower Akt phosphorylation in NK cells cultured with IL-15 and NAM was associated with higher FOXO1 protein and reduced proteasomal degradation. Consequently, FOXO1 was enriched within the proximal promoter of *SELL* for enhanced transcription and CD62L stability that was maintained in vivo after NAM withdrawal. CD62L binds high endothelial venules in lymph nodes and Peyer′s patches through recognition of endothelial glycoproteins and the mucosal vascular addressin MAdCAM-1 (*26*, *27*). Human CD62L$^+$ NKT cells have superior in vivo persistence and antitumor function relative to CD62L$^-$ NKT cells and exhibit a less differentiated gene expression profile (*28*). This is in line with our findings that NK cells cultured with IL-15 and NAM, which have elevated CD62L, persisted at higher frequencies in multiple tissues after adoptive transfer and had a transcriptional profile mirroring immature CD56^{bright} NK cells. NK cells cultured with IL-15 and NAM had elevated expression of fucosyltransferase 7 (*FUT7*), which is involved in the last step of sialyl Lewis X determinant synthesis (*29*). Sialyl Lewis X determinant, which is the specific carbohydrate ligand for selectins, is constitutively expressed or induced upon activation by multiple immune cell types and mediates inflammatory extravasation of cells (*30*, *31*). Higher CD62L, CD44, and FUT7 in NK cells cultured with NAM suggests enhanced capacity for homing to lymph nodes and sites of inflammation. However, we were unable to test this directly because of the lack of secondary lymphoid tissue in NSG mice. The development of better xenogeneic models will be necessary to study human lymphocyte homing.

In the phase 1 dose escalation trial of NAM-expanded allogeneic NK cells (GDA-201) in combination with rituximab for the treatment of R/R DLBCL and FL, 16 of the 20 patients enrolled received the maximum target dose of cells. Among the 19 patients evaluable for response, 13 patients (65%) had a CR, and 1 patient had a PR, for a best OR rate of 74%. Overall survival at 2 years was 73% with a median duration of response of 16 months. These are comparable to CD19 chimeric antigen receptor (CAR)–T therapies where OR rates of 60 to 70% and 2-year PFS of 40% have been reported (*32*). They are also comparable to cord blood–derived allogeneic CD19 CAR-NK cell therapy where 8 of 11 evaluable patients had an objective response and 7 patients achieved a CR (*33*). Our prior experience using donor NK cells without NAM expansion showed lower clinical efficacy (OR rate of 30%) for a similar high-risk lymphoma population (*5*). One question is to what extent NAM-expanded NK cells contributed to the clinical response in this trial. This question would best be answered by including a comparison group lacking NK cell adoptive transfer. However, the small size of this phase 1 trial did not allow for additional groups. Results from a historical study of rituximab, fludarabine, and mitoxantrone chemotherapy in patients with R/R FL and mantle cell lymphoma demonstrated antitumor activity but required multiple cycles of chemo-immunotherapy. The CR (33%) and PR (45%) rates were low, and the duration of responses was brief (*34*). Although our study had a similar OR rate, we observed higher CR rates and longer PFS duration, suggesting a potential added benefit of NAM-expanded NK cell adoptive transfer. GDA-201 cells outnumbered recipient NK cells in the peripheral blood of most patients at peak numbers and were detected up to 10 to 14 days after infusion. These cells were also detected in tumor biopsies after infusion. Furthermore, the post–GDA-201 infusion tumor biopsies demonstrated cancer cell necrosis with evidence of scattered NK cells and a dense T cell infiltrate. This finding suggests potential cooperation between GDA-201 and the adaptive arm of host immunity. Further studies will be needed to explore this hypothesis. This

trial showed that GDA-201 can be administered safely without immune-mediated toxicities or severe cytopenia.

A limitation of this study was the lack of available lymph node biopsy tissue from a nonresponding patient with CODEX imaging for comparison of NK and T cell infiltration. Future prospective clinical studies designed to image various immune populations before and after adoptive transfer in responding and nonresponding patients will be needed to determine the role of NK cells more definitively in recruiting T cells to the tumor site. Although the clinical response rates in this study compare favorably with anti-CD19 CAR-T cell treatment of DLBCL (*32*), another limitation of this study is the relatively small cohort size. A larger phase 2 study testing a cryopreserved formulation of GDA-201 for the treatment of aggressive and indolent NHL is underway to validate and extend the present findings. The universal potential for GDA-201 with cancer antigen–targeting monoclonal antibodies may be explored for other malignancies.

MATERIALS AND METHODS

Study design

Patients with R/R MM or NHL have poor prognoses, and cell therapy is a promising approach to yield durable remissions. This phase 1 study explored the safety and feasibility of ex vivo HLA-haploidentical or HLA-mismatched NAM-expanded NK cell adoptive therapy (GDA-201) after lymphodepleting chemotherapy and in combination with targeted monoclonal antibodies, followed by a short course of IL-2 to facilitate NK cell survival and expansion in vivo. We hypothesized that infusion of GDA-201 would be safe and result in tumor control in patients with NHL and MM. Randomization and blinding were not applicable. All enrolled patients voluntarily signed institutional review board–approved informed consent to be treated in the first-in-human phase 1 dose escalation trial of GDA-201 (NCT03019666). The primary objectives of this clinical trial were to evaluate the safety and efficacy of GDA-201 in patients with R/R NHL. A synopsis with inclusion and exclusion criteria is included in the Supplementary Materials. Eligible patients were above the age of 18 with $CD20^+$ B cell NHL or MM who failed conventional therapy and had HLA haploidentical or mismatched related donors. Patients received three doses of rituximab (375 mg/m^2) and lymphodepleting chemotherapy consisting of cyclophosphamide (400 mg/m^2 × one dose) and fludarabine (30 mg/m^2 × three doses) followed by GDA-201 and subcutaneous doses of IL-2 (6×10^6 units) at days 0, 2, and 4 to support NK cell survival in vivo. For manufacturing of GDA-201, PBMCs were collected from donors by apheresis, and T cells were removed via anti-CD3 magnetic depletion. Cells were then cultured for 14 days with IL-15 (20 ng/ml) and NAM (5 mM) in the GMP facility at the University of Minnesota, washed, and infused into patients intravenously. Sixteen patients received the maximum target dose of 2×10^8 cells. The primary end points included safety, dose-limiting toxicities, OR rates, CR rates, PR rates, duration of responses, PFS, and overall survival. The time-to-event continual reassessment method was used to establish the GDA-201 dose that was safe and most closely corresponded to a target rate of dose-limiting toxicity of 15%. Three dose levels were tested (2×10^7, 10×10^7, and 2×10^8/kg GDA-201 cells given on days 0 and +2) with cohorts of two patients per dose. Once the phase 1 study was completed, enrollment continued in an expansion phase until 10 patients with NHL and 10 patients with MM, including any patients treated at the maximum tolerated dose (MTD) during the phase 1 trial, were treated at the highest tolerated GDA-201 dose level. Each disease group accrued independently, with enrollment closed once all 10 evaluable patients were enrolled at the MTD.

Cell isolation and culture

Peripheral blood products were obtained from the Memorial Blood Bank (Minneapolis, MN). PBMCs were isolated by Ficoll-Paque (GE Healthcare) density gradient centrifugation. T and B cells were depleted using anti-CD3 and anti-CD19 magnetic beads (STEMCELL Technologies). CD3/CD19-depleted cells were cultured in B0 media [Dulbecco's modified Eagle's medium plus Ham's F-12 medium, 2:1, supplemented with 10% heat-inactivated human AB sera, 1% penicillin-streptomycin, 25 mM β-mercaptoethanol, ascorbic acid (20 mg/ml), and sodium selenite (0.05 mg/ml)] with IL-15 (10 ng/ml; National Cancer Institute). In NAM-supplemented cultures, 5 mM NAM (Sigma-Aldrich) was added. In some experiments, NK cells were isolated using the EasySep Human NK Cell Isolation Kit (STEMCELL Technologies). In experiments testing FOXO1 inhibition, 100 nM AS1842856 (Sigma-Aldrich) was added at the beginning of culture. In experiments assessing FOXO1 stabilization, cycloheximide (10 mg/ml; Sigma-Aldrich) and 10 mM MG132 (Sigma-Aldrich) were used. In experiments testing the effect of NAM on CD62L and CD16 surface cleavage, IL-12 (10 ng/ml; R&D Systems), IL-18 (100 ng/ml; R&D Systems), and BMS56634 (10 μg/ml; Bristol Myers Squibb) were added to overnight cultures. For the clinical trial, peripheral blood was collected to obtain mononuclear cells by density gradient centrifugation. Flow cytometry and chimerism studies were performed with fresh cells.

Flow cytometry and cell sorting

Staining was performed with fluorochrome-conjugated antibodies against CD3 (OKT3; RRID: AB_2904343), CD56 (HNCD56; RRID:AB_604095), KIR2DL1 (HP-MA4; RRID:AB_2130376), KIR2DL2/3 (DX27; RRID:AB_2296485), KIR3DL1 (DX9; RRID:AB_314946), CD57 (QA17AM; RRID:AB_2860965), CD16 (3G8; RRID:AB_2616616), NKp30 (P30-15; RRID:Ab_2810489), NKp46 (9E2; RRID:AB_2561649), 2B4 (C1.7; RRID:AB_1279188), LFA-1 (m24; RRID:AB_2565288), CD62L (DREG-56; RRID:AB_314469), CD44 (BJ18; RRID:AB_1501202), CD107a (H4A3; RRID:AB_1186058), TNF (Mab11; RRID:AB_2561315), IFN-γ (4S.B3; RRID:AB_10900083) (all from BioLegend), pAkt-S473 (D9E, Cell Signaling Technology), pSTAT5-Y694 (BD Biosciences; RRID:AB_399881), pFOXO1-S256 (Thermo Fisher Scientific), NKG2A (Z199, Beckman Coulter), CD2 (RPA-2.10, BD Biosciences; RRID:_AB396481), HLA-A24 (K0209-4, MBL; RRID:AB_592234), HLA-Bw4 (REA274, Miltenyi; RRID:AB_2652010), HLA-B7 (BB7.1, Thermo Fisher Scientific), HLA-B12 (130-099-862, Miltenyi; RRID:AB_2652097), HLA-B8 (130-099-583, Miltenyi; RRID:AB_2652004), HLA-A2 (BB7.2, BioLegend; RRID:AB_1659246), and HLA-A3 (GAP.A3, BD Biosciences; RRID_AB2872241). In some experiments, NK cells were stained with MitoSOX Red Mitochondrial Superoxide Indicator dye (Thermo Fisher Scientific). Cells were surface-stained with dead cell stain (Thermo Fisher Scientific) in fluorescence-activated cell sorting (FACS) buffer [phosphate-buffered saline (PBS) supplemented with 2% fetal bovine serum and 2 mM EDTA] and fixed in

2% formaldehyde. Flow data were acquired on LSR II (BD Biosciences) and analyzed with FlowJo software, v10 (BD Biosciences). Cell sorting was performed using FACSAria (BD Biosciences).

Western blots and confocal microscopy

For Western blots, cells were lysed and run on 10% SDS–polyacrylamide gel electrophoresis gels. Proteins were then transferred to nitrocellulose membranes, which were incubated overnight with primary antibodies against FOXO1 (C29H4, Cell Signaling Technology), Akt 1/2/3 (5C10, Santa Cruz Biotechnology; RRID:AB_1118808), pAkt-Ser^{473} (D9E, Cell Signaling Technology), and ubiquitin (A-5, Santa Cruz Biotechnology; RRID:AB_2241297) at a dilution of 1:1000. Membranes were washed and incubated with anti-rabbit or anti-mouse horseradish peroxidase secondary antibodies at a 1:2000 dilution for 1 hour. Immunoreactive bands were imaged on a UVP Imaging System with enhanced chemiluminescence reagents (Thermo Fisher Scientific). Densitometry analyses were performed using ImageJ software (National Institutes of Health). For imaging experiments, cells were stained with the same FOXO1 antibody used for Western blot. After staining, cells were washed with PBS and spun onto slides with Cytospin 2 (Shandon). Cells were fixed and mounted in Vectashield with 4′,6-diamidino-2-phenylindole staining dye (Vector Laboratories). Images were acquired with an Olympus BX upright microscope (Olympus). Image processing was performed using Icy open platform software.

Quantitative RT-PCR and ChIP

For quantification of gene expression, cells were lysed in RLT buffer (Qiagen), and RNA was extracted using the RNeasy Plus Micro Kit (Qiagen). Complementary DNA was synthesized using SuperScript IV Reverse Transcriptase (Thermo Fisher Scientific). qRT-PCRs were performed using SYBR Green PCR Master Mix (Applied Biosystems). Primer sequences are as follows: *SELL*, 5′-AGCCCTCT GTTACACAGCTTC-3′ (forward) and 5′-ACCCCACATCACAGT TGCAG-3′ (reverse); *FOXO1*, 5′-GGGTTAGTGAGCAGGTTA CAC-3′ (forward) and 5′-ACTAAAAGGGAGTTGGTGAAA GACA-3′ (reverse); and *ACTB*, 5′-CACACTGTGCCCATCTACG A-3′ (forward) and 5′-GCCATCTCTTGCTCGAAGTC-3′ (reverse). Gene expression analyses were normalized against *ACTB*. For ChIP assays, aliquots of 2.5×10^6 formaldehyde-fixed cells were resuspended in 50 ml of nuclei isolation buffer (Abcam). Chromatin was digested by adding 15 U of MNase (Thermo Fisher Scientific) and incubating at 37°C for 5 min. EDTA was added to stop the reactions. Digested chromatin was diluted in immunoprecipitation buffer with EDTA-free protease inhibitors (Millipore) and precleared with protein G agarose (Millipore) for 1 hour at 4°C. Precleared chromatin was immunoprecipitated overnight at 4°C with an antibody against FOXO1 (3B6, Invitrogen). Samples were then washed and eluted, and cross-links were reversed with a 4-hour incubation at 65°C. DNA was precipitated and analyzed by qRT-PCR.

Metabolic and in vitro function assays

For metabolite quantification, the NAD/NADH Quantitation Kit, NADP/NADPH Quantitation Kit, and ATP Bioluminescence Assay Kit HSII (all from Millipore) were used. Mass spectrometry and data analysis for principal metabolite quantification were performed by Metabolon. For assays testing NK cell oxidative stress, cells were incubated at 37°C for 1 hour with or without 100 mM H_2O_2 (Sigma-Aldrich). For glucose tracing experiments, NK cells cultured with and without NAM were washed and resuspended in media containing 0.5 M $^{13}C_6$ glucose (Sigma-Aldrich) for 1 hour. Carbon-labeled acetyl-CoA was analyzed by liquid chromatography–tandem mass spectrometry (LC/MS/MS) using an UltiMate 3000 Quaternary UHPLC coupled to a Q-Exactive Plus mass spectrometer (Thermo Fisher Scientific). Real-time metabolic flux analyses were performed using the Seahorse XF Glycolysis Stress Test Kit and the Seahorse XF Cell Mito Stress Test Kit (both from Agilent). Cells were analyzed with a Seahorse Xfe96 Analyzer instrument (Agilent). For flow cytometry–based function assays, NK cells were incubated with K562 cells [CRL-3343, American Type Culture Collection (ATCC)] or Raji cells (CCL-86, ATCC) with or without rituximab (1 μg/ml) (Genentech). After 4 hours of coincubation, intracellular and surface staining was performed using antibodies listed above. For intracellular staining, GolgiStop and GolgiPlug (BD Biosciences) were used to block cytokine secretion. Cells were permeabilized in 0.05% Triton X-100 (Millipore). For IncuCyte assays, NK cells were cocultured with K562 cells transduced with NucLight Red (Essen Bioscience) and analyzed with the IncuCyte S3 Live-Cell Analysis System (Essen Bioscience).

In vivo xenogeneic adoptive transfer experiments

For all animal experiments, 6- to 8-week-old female NSG mice (Jackson Laboratory, strain no. 001303) were used. All experiments were reviewed and approved by the University of Minnesota Animal Care Committee under the protocol 1907-37257A. For experiments assessing the stability of CD62L after NAM withdrawal, 5×10^6 NK cells cultured with or without NAM were injected into the peritonea of NOD *scid* gamma (NSG) mice. Groups of mice were sacrificed at days 7 and 14. Peritoneal washes were performed to collect cells, and CD62L expression on human NK cells was assessed by flow cytometry. For experiments analyzing NK cell tissue retention, NK cells cultured with and without NAM were labeled with CFSE dye (Thermo Fisher Scientific) and injected intravenously into NSG mice (1.5×10^7 cells per mouse). Control mice received injections of buffer alone. Mice were sacrificed after 4 days, and blood, bone marrow, and spleen tissues were harvested for assessment of frequencies of adoptively transferred cells by flow cytometry.

Lymph node immunohistochemistry

The samples of lymph nodes were obtained by radiologic imaging–guided core needle biopsy. The tissues were fixed in 10% formalin and processed into paraffin blocks. Five-micrometer-thick sections were stained with hematoxylin-eosin or immunohistochemical stains performed using a Ventana Benchmark stainer with antibodies specific for CD20 (L26, Roche) and CD3 (2GV6, Roche). The microscopic images were taken using an Olympus BX46 microscope with an Olympus DP74 camera.

Single-cell and bulk RNA-seq

For scRNA-seq experiments, NK cells were sorted from banked aliquots of clinical apheresis products and GDA-201 NK cells expanded at the GMP cell therapy facility at the University of Minnesota using antibodies against CD56 and CD3 to distinguish the NK cell populations. Day 4 GDA-201 and host NK cells were sorted from banked patient peripheral blood using antibodies against CD56, CD3, HLA-A2, and HLA-A3. Day 4 GDA-201 cells

were HLA-A2/3 positive, whereas host NK cells were HLA-A2/3 negative. For scRNA-seq, sorted NK cells were washed in Dulbecco's PBS + 0.04% bovine serum albumin and submitted to the University of Minnesota Genomics Center for sample preparation and sequencing. Briefly, we used the Chromium Single Cell 3′ Reagent Kit (v3 Chemistry) for library preparation (10X Genomics). Libraries were sequenced on NovaSeq 6000 (Illumina), and raw FASTQ files were processed with CellRanger software v4.0.0 (10X Genomics) for read alignment, barcode counting, and unique molecular identifier counting. Reads were aligned and mapped to the GRch38 sequence, and low-quality cells were removed from the analysis. Log normalization was performed on gene expression values for further downstream analysis. For bulk RNA-seq, $CD56^{bright}$, $CD56^{dim}$ $CD94^{high}$, and $CD56^{dim}CD94^{low/-}$ NK cells were sorted from peripheral blood from four healthy donors. RNA was extracted using the RNeasy Plus Micro Kit (Qiagen). Barcoded TruSeq RNA v2 libraries (Illumina) were created and sequenced on HiSeq 2500 (Illumina) as paired-end 100–base pair reads. RNA-seq reads were aligned to GRch38, and raw read counts were processed by R (version 3.2.0) and subjected to normalization and differential expression analysis in the R/Bioconductor package.

Statistical analyses

All statistics were calculated with GraphPad Prism (v9.0). Data are expressed as the mean ± SEM. Differences between groups were determined by Student's *t* tests, one-way analysis of variance (ANOVA), or mixed-effects analyses. *P* values of <0.05 were considered statistically significant. For RNA-seq, *P* values were determined using Wilcoxon tests. Uncertainty is represented by error bars in the figures as SEM. Statistical analyses used for the clinical trial are summarized in Supplementary Materials and Methods.

Supplementary Materials

This PDF file includes:
Materials and Methods
Figs. S1 to S6
Tables S1 to S4

Other Supplementary Material for this manuscript includes the following:
Data file S1
MDAR Reproducibility Checklist

View/request a protocol for this paper from *Bio-protocol*.

REFERENCES AND NOTES

1. E. Narni-Mancinelli, S. Ugolini, E. Vivier, Tuning the threshold of natural killer cell responses. *Curr. Opin. Immunol.* **25**, 53–58 (2013).
2. J. S. Miller, Y. Soignier, A. Panoskaltsis-Mortari, S. A. McNearney, G. H. Yun, S. K. Fautsch, D. McKenna, C. Le, T. E. Defor, L. J. Burns, P. J. Orchard, B. R. Blazar, J. E. Wagner, A. Slungaard, D. J. Weisdorf, I. J. Okazaki, P. B. McGlave, Successful adoptive transfer and in vivo expansion of human haploidentical NK cells in patients with cancer. *Blood* **105**, 3051–3057 (2005).
3. V. Bachanova, S. Cooley, T. E. Defor, M. R. Verneris, B. Zhang, D. H. McKenna, J. Curtsinger, A. Panoskaltsis-Mortari, D. Lewis, K. Hippen, P. McGlave, D. J. Weisdorf, B. R. Blazar, J. S. Miller, Clearance of acute myeloid leukemia by haploidentical natural killer cells is improved using IL-2 diphtheria toxin fusion protein. *Blood* **123**, 3855–3863 (2014).
4. V. Bachanova, D. Sarhan, T. E. DeFor, S. Cooley, A. Panoskaltsis-Mortari, B. R. Blazar, J. M. Curtsinger, L. Burns, D. J. Weisdorf, J. S. Miller, Haploidentical natural killer cells induce remissions in non-Hodgkin lymphoma patients with low levels of immune-suppressor cells. *Cancer Immunol. Immunother.* **67**, 483–494 (2018).
5. T. Peled, H. Shoham, D. Aschengrau, D. Yackoubov, G. Frei, G. N. Rosenheimer, B. Lerrer, H. Y. Cohen, A. Nagler, E. Fibach, A. Peled, Nicotinamide, a SIRT1 inhibitor, inhibits differentiation and facilitates expansion of hematopoietic progenitor cells with enhanced bone marrow homing and engraftment. *Exp. Hematol.* **40**, 342–355.e1 (2012).
6. R. N. Mohammed, H. A. Watson, M. Vigar, J. Ohme, A. Thomson, I. R. Humphreys, A. Ager, L-Selectin is essential for delivery of activated $CD8^+$ T cells to virus-infected organs for protective immunity. *Cell Rep.* **14**, 760–771 (2016).
7. H. C. DeGrendele, P. Estess, M. H. Siegelman, Requirement for CD44 in activated T cell extravasation into an inflammatory site. *Science* **278**, 672–675 (1997).
8. J. J. Peschon, J. L. Slack, P. Reddy, K. L. Stocking, S. W. Sunnarborg, D. C. Lee, W. E. Russell, B. J. Castner, R. S. Johnson, J. N. Fitzner, R. W. Boyce, N. Nelson, C. J. Kozlosky, M. F. Wolfson, C. T. Rauch, D. P. Cerretti, R. J. Paxton, C. J. March, R. A. Black, An essential role for ectodomain shedding in mammalian development. *Science* **282**, 1281–1284 (1998).
9. R. Romee, B. Foley, T. Lenvik, Y. Wang, B. Zhang, D. Ankarlo, X. Lou, S. Cooley, M. R. Verneris, B. Walcheck, J. S. Miller, NK cell CD16 surface expression and function is regulated by a disintegrin and metalloprotease-17 (ADAM17). *Blood* **121**, 3599–3608 (2013).
10. Y. M. Kerdiles, D. R. Beisner, R. Tinoco, A. S. Dejean, D. H. Castrillon, R. A. DePinho, S. M. Hedrick, Foxo1 links homing and survival of naive T cells by regulating L-selectin, CCR7 and interleukin 7 receptor. *Nat. Immunol.* **10**, 176–184 (2009).
11. Y. Deng, Y. Kerdiles, J. Chu, S. Yuan, Y. Wang, X. Chen, H. Mao, L. Zhang, J. Zhang, T. Hughes, Y. Deng, Q. Zhang, F. Wang, X. Zou, C.-G. Liu, A. G. Freud, X. Li, M. A. Caligiuri, E. Vivier, J. Yu, Transcription factor Foxo1 is a negative regulator of natural killer cell maturation and function. *Immunity* **42**, 457–470 (2015).
12. S. M. Hedrick, R. H. Michelini, A. L. Doedens, A. W. Goldrath, E. L. Stone, FOXO transcription factors throughout T cell biology. *Nat. Rev. Immunol.* **12**, 649–661 (2012).
13. Y. Lou, X. Lu, X. Dang, FOXO1 up-regulates human Lselectin expression through binding to a consensus FOXO1 motif. *Gene Regul. Syst. Bio.* **6**, 139–149 (2012).
14. S. J. Mitchell, M. Bernier, M. A. Aon, S. Cortassa, E. Y. Kim, E. F. Fang, H. H. Palacios, A. Ali, I. Navas-Enamorado, A. Di Francesco, T. A. Kaiser, T. B. Waltz, N. Zhang, J. L. Ellis, P. J. Elliott, D. W. Frederick, V. A. Bohr, M. S. Schmidt, C. Brenner, D. A. Sinclair, A. A. Sauve, J. A. Baur, R. de Cabo, Nicotinamide improves aspects of healthspan, but not lifespan, in mice. *Cell Metab.* **27**, 667–676.e4 (2018).
15. W. Xiao, R.-S. Wang, D. E. Handy, J. Loscalzo, NAD(H) and NADP(H) redox couples and cellular energy metabolism. *Antioxid. Redox Signal.* **28**, 251–272 (2018).
16. A. E. Pegg, Functions of polyamines in mammals. *J. Biol. Chem.* **291**, 14904–14912 (2016).
17. J. Muri, M. Kopf, Redox regulation of immunometabolism. *Nat. Rev. Immunol.* **21**, 363–381 (2021).
18. F. Cichocki, C.-W. Wu, B. Zhang, M. Felices, B. Tesi, K. Tuininga, P. Dougherty, E. Taras, P. Hinderelie, B. R. Blazar, Y. T. Bryceson, J. S. Miller, ARID5B regulates metabolic programming in human adaptive NK cells. *J. Exp. Med.* **215**, 2379–2395 (2018).
19. R. A. Cairns, T. W. Mak, The current state of cancer metabolism. *Nat. Rev. Cancer* **16**, 613–614 (2016).
20. H. Sies, C. Berndt, D. P. Jones, Oxidative stress. *Annu. Rev. Biochem.* **86**, 715–748 (2017).
21. P. Korge, G. Calmettes, J. N. Weiss, Increased reactive oxygen species production during reductive stress: The roles of mitochondrial glutathione and thioredoxin reductases. *Biochim. Biophys. Acta* **1847**, 514–525 (2015).
22. A. Stincone, A. Prigione, T. Cramer, M. M. C. Wamelink, K. Campbell, E. Cheung, V. Olin-Sandoval, N. M. Grüning, A. Krüger, M. T. Alam, M. A. Keller, M. Breitenbach, K. M. Brindle, J. D. Rabinowitz, M. Ralser, The return of metabolism: Biochemistry and physiology of the pentose phosphate pathway. *Biol. Rev. Camb. Philos. Soc.* **90**, 927–963 (2015).
23. Y. Wang, F. Wang, L. Wang, S. Qiu, Y. Yao, C. Yan, X. Xiong, X. Chen, Q. Ji, J. Cao, G. Gao, D. Li, L. Zhang, Z. Guo, R. Wang, H. Wang, G. Fan, NAD^+ supplement potentiates tumor-killing function by rescuing defective TUB-mediated NAMPT transcription in tumor-infiltrated T cells. *Cell Rep.* **36**, 109516 (2021).
24. A. Y. Mah, A. Rashidi, M. P. Keppel, N. Saucier, E. K. Moore, J. B. Alinger, S. K. Tripathy, S. K. Agarwal, E. K. Jeng, H. C. Wong, J. S. Miller, T. A. Fehniger, E. M. Mace, A. R. French, M. A. Cooper, Glycolytic requirement for NK cell cytotoxicity and cytomegalovirus control. *JCI Insight* **2**, e95128 (2017).
25. D. Bridge, A. G. Theofiles, R. L. Holler, E. Marcinkevicius, R. E. Steele, D. E. Martínez, FoxO and stress responses in the cnidarian Hydra vulgaris. *PLOS ONE* **5**, e11686 (2010).
26. S. Baumheter, M. S. Singer, W. Henzel, S. Hemmerich, M. Renz, S. D. Rosen, L. A. Lasky, Binding of L-selectin to the vascular sialomucin CD34. *Science* **262**, 436–438 (1993).
27. E. L. Berg, L. M. McEvoy, C. Berlin, R. F. Bargatze, E. C. Butcher, L-Selectin-mediated lymphocyte rolling on MAdCAM-1. *Nature* **366**, 695–698 (1993).
28. G. Tian, A. N. Courtney, B. Jena, A. Heczey, D. Liu, E. Marinova, L. Guo, X. Xu, H. Torikai, Q. Mo, G. Dotti, L. J. Cooper, L. S. Metelitsa, $CD62L^+$ NKT cells have prolonged persistence and antitumor activity in vivo. *J. Clin. Invest.* **126**, 2341–2355 (2016).

29. S. Natsuka, K. M. Gersten, K. Zenita, R. Kannagi, J. B. Lowe, Molecular cloning of a cDNA encoding a novel human leukocyte α-1,3-fucosyltransferase capable of synthesizing the sialyl Lewis x determinant. *J. Biol. Chem.* **269**, 16789–16794 (1994).
30. M. L. Phillips, E. Nudelman, F. C. Gaeta, M. Perez, A. K. Singhal, S. Hakomori, J. C. Paulson, ELAM-1 mediates cell adhesion by recognition of a carbohydrate ligand, sialyl-Lex. *Science* **250**, 1130–1132 (1990).
31. K. Ohmori, F. Fukui, M. Kiso, I. Imai, O. Yoshie, H. Hasegawa, K. Matsushima, R. Kannagi, Identification of cutaneous lymphocyte-associated antigen as sialyl 6-sulfo Lewis X, a selectin ligand expressed on a subset of skin-homing helper memory T cells. *Blood* **107**, 3197–3204 (2006).
32. S. J. Schuster, M. R. Bishop, C. S. Tam, E. K. Waller, P. Borchmann, J. P. McGuirk, U. Jäger, S. Jaglowski, C. Andreadis, J. R. Westin, I. Fleury, V. Bachanova, S. R. Foley, P. J. Ho, S. Mielke, J. M. Magenau, H. Holte, S. Pantano, L. B. Pacaud, R. Awasthi, J. Chu, Ö. Anak, G. Sales, R. T. Maziarz; JULIET Investigators, Tisagenlecleucel in adult relapsed or refractory diffuse large B-cell lymphoma. *N. Engl. J. Med.* **380**, 45–56 (2019).
33. E. Liu, D. Marin, P. Banerjee, H. A. Macapinlac, P. Thompson, R. Basar, L. N. Kerbauy, B. Overman, P. Thall, M. Kaplan, V. Nandivada, I. Kaur, A. N. Cortes, K. Cao, M. Daher, C. Hosing, E. N. Cohen, P. Kebriaei, R. Mehta, S. Neelapu, Y. Nieto, M. Wang, W. Wierda, M. Keating, R. Champlin, E. J. Shpall, K. Rezvani, Use of CAR-transduced natural killer cells in CD19-positive lymphoid tumors. *N. Engl. J. Med.* **382**, 545–553 (2020).
34. R. Forstpointer, M. Dreyling, R. Repp, S. Hermann, A. Hänel, B. Metzner, C. Pott, F. Hartmann, F. Rothmann, R. Rohrberg, H. P. Böck, H. Wandt, M. Uterhalt, W. Hiddemann; German Low-Grade Lymphoma Study Group, The addition of rituximab to a combination of fludarabine, cyclophosphamide, mitoxantrone (FCM) significantly increases the response rate and prolongs survival as compared with FCM alone in patients with relapsed and refractory follicular and mantle cell lymphomas: Results of a prospective randomized study of the German Low-Grade Lymphoma Study Group. *Blood* **104**, 3064–3071 (2004).

Acknowledgments
Funding: This work was supported by NIH R01 HL155150 (to F.C.), NIH P01 CA111412 (to J.S.M.), NIH P01 CA65493 (to J.S.M.), NIH R35 CA197292 (to J.S.M.), and research funds provided by Gamida Cell Ltd. (to V.B. and F.C.). The clinical trial (NCT03019666) was an investigator-initiated trial and fully sponsored by Gamida Cell Ltd. (principal investigator: V.B.). **Author contributions:** F.C., Y.G., J.H., J.S.M., and V.B. conceptualized, designed, and supervised the study. B.Z., C.-Y.W., E.C., A.D., A.K., R.S.O., D.Y., and R.S. performed research and developed methodology. F.C. and V.B. analyzed data. D.H.M., M.J., R.W., Z.C., B.G., and J.M. supervised and performed studies related to the clinical trial. Q.C. and T.E.D. provided statistical support. F.C. and V.B. wrote the manuscript. All authors have critically reviewed the manuscript. **Competing interests:** F.C. and J.S.M. are paid consultants for Fate Therapeutics, and they receive research funds and stock options from this relationship. J.S.M. serves on the Scientific Advisory Board of ONK Therapeutics and Wugan and is a paid consultant for GT BioPharma and Vycellix (with research funds and stock options), all unrelated to the content of this manuscript. M.J. receives consulting fees from Jansen. B.G. is a paid consultant for Fate Therapeutics and MLM Diagnostics. R.S.O. receives equity from Nucleus Biologics, research support from NeoTx, and patent licensing from Novartis. These relationships are unrelated to the content of this manuscript. F.C. and V.B. receive research and clinical trial financial support from Gamida Cell Ltd. V.B. serves on the DSMB for Miltenyi Biotech and on advisory boards for AstraZeneca, Amgen, Kite, ADC Therapeutics, and Takeda. V.B. also receives research funding from Citius and Incyte. D.Y., R.S., and Y.G. are employees of Gamida Cell Ltd. **Data and materials availability:** All data associated with this study are present in the paper or the Supplementary Materials. RNA-seq data can be found under the GEO accession number GSE222369. Reagents and other research materials are available from the University of Minnesota via material transfer agreement upon request.

Submitted 9 August 2022
Resubmitted 16 January 2023
Accepted 29 June 2023
Published 19 July 2023
10.1126/scitranslmed.ade3341

Science Translational Medicine

Nicotinamide enhances natural killer cell function and yields remissions in patients with non-Hodgkin lymphoma

Frank Cichocki, Bin Zhang, Cheng-Ying Wu, Emily Chiu, Abderrahman Day, Roddy S. OConnor, Dima Yackoubov, Ronit Simantov, David H. McKenna, Qing Cao, Todd E. Defor, Murali Janakiram, Rose Wangen, Zuzan Cayci, Nathaniel Snyder, Akhilesh Kumar, Bartosz Grzywacz, Justin Hwang, Yona Geffen, Jeffrey S. Miller, Joseph Maakaron, and Veronika Bachanova

Sci. Transl. Med., **15** (705), eade3341.
DOI: 10.1126/scitranslmed.ade3341

Science Translational Medicine (ISSN) is published by the American Association for the Advancement of Science. 1200 New York Avenue NW, Washington, DC 20005. The title *Science Translational Medicine* is a registered trademark of AAAS.